Importance of particle formation to reconstructed water column biogenic silica fluxes

by

Moriceau, Brivaëla, Gallinari, Morgane, Soetaert, Karline, Ragueneau, Olivier

UMR CNRS 6539, Institut Universitaire Européen de la Mer, Place Copernic,
Technopôle Brest-Iroise, 29280 Plouzané, France

Running title: Reconstruction of $bSiO_2$ fluxes from dissolution experiments

Revised manuscript to be submitted (April 2007) to

Global Biogeochemical Cycles

Key Words: Biogenic silica fluxes, dissolution, aggregate, modelling

Manuscript submitted:

1) Revised version of ms submitted: _____

2) Manuscript eventually accepted: _____

For correspondence:

Brivaëla MORICEAU

UMR 6539, Institut Universitaire Européen de la Mer
Technopole Brest-Iroise, Place Nicolas Copernic
F – 29280 Plouzané, France
Tel: ++33 2.98.49.88.99 · Fax: ++33 2.98.49.86.45
E-mail: moriceau@univ-brest.fr

Abstract

The particles sinking out of the ocean's surface layer are made up of a mixture of living and dead algal cells, fecal pellets and aggregates, while the parameters used to describe the behaviour of biogenic silica ($bSiO_2$) in today's models are experimentally determined on freely suspended diatoms (FC). In a simple advection-reaction model we combine sinking rates of FC, zooplankton fecal pellets and aggregates with recent measurements of $bSiO_2$ dissolution to reconstruct theoretical downward profiles of $bSiO_2$ fluxes at 8 sites in the world ocean. Statistical analyses showed that sinking and dissolution parameters for two pools of $bSiO_2$ are required to model particle fluxes accurately. The 2-pool model results confirm the importance of seasonality for particle formation and its connection to the percentage of the $bSiO_2$ production that reaches the seafloor. The depth of $bSiO_2$ recycling appears to be influenced more by particle formation than by dissolution rates of $bSiO_2$ or the ballast effect of the dense diatom frustules.

1. Introduction

Diatoms form the basis of a short food chain that leads to carbon export to higher trophic levels [*Cushing*, 1989; *Thornton*, 2002] and to deeper waters [*Buesseler*, 1998]. They are an important player in the global carbon cycle because of their participation in an efficient food web and their ability to aggregate [*Smetacek*, 1999]. Because diatoms require silica to build their frustules, their share in total primary production (PP) depends on the availability of the nutrient silicic acid (DSi) in many regions of the world ocean such as the equatorial Pacific [*Dugdale et al.*, 1995; *Leynaert et al.*, 2001] or the Southern Ocean [*Brzezinski et al.*, 2001; *Pondaven et al.*, 1998]. The availability of DSi in surface waters, in particular relative to other nutrients, is linked to the composition of the source waters in upwelling regions and/or the intensity of biogenic silica ($bSiO_2$) recycling in surface waters in other oceanic regions. Depending on the depth of $bSiO_2$ dissolution, diatom production is affected on different time scale. Shallow depth mineralization immediately influences diatom production and phytoplankton dynamics [*Officer and Ryther*, 1980]. Recycling in intermediate waters [*Sarmiento et al.*, 2004] and/or deep waters [*Ragueneau et al.*, 2000] affects the meridional distribution of DSi or the redistribution of DSi among oceanic basins, respectively, with implications for intermediate to long time scales.

A global average of 60% of the $bSiO_2$ produced in surface waters is recycled in the first 100 m [*Nelson et al.*, 1995; *Tréguer et al.*, 1995]. This global mean hides large regional differences [*Nelson et al.,* 1995; *Ragueneau et al.,* 2000, 2002], which can not be related to any simple trend in production or diatom abundance, nor to any single mechanism known to influence dissolution, such as temperature [*Lawson et al.*, 1978] or bacterial activity [*Bidle and Azam*, 1999]. The dissolution to production ratio, integrated over the surface layer ($\int D:\int P$), has been related to the formation of diatom blooms by *Brzezinski et al.* [2003]; this ratio is lower during blooms, leaving more room for export and deeper recycling. However, the use of global biogeochemical models to reproduce both DSi and $bSiO_2$ flux profiles in the global ocean is difficult and does

not always agree with in situ measurements [*Aumont et al*., 2003]. We hypothesize that the present difficulty in modeling both the $bSiO_2$ and DSi profiles of the global ocean are due to underestimating the importance of particle formation. Whereas aggregates and fecal pellets of large grazers are major vehicles for export [review in *Turner,* 2002 and *Thornton,* 2002], the parameters used to represent the fate of PP in global ocean models are still measured on freely suspended diatoms.

To test this hypothesis, we developed a simple advection-reaction model using one and then two different pools of particles. The model combines a series of in vitro $bSiO_2$ dissolution experiments undertaken on the different constituents of the flux: freely suspended diatoms [compiled in *Van Cappellen et al.*, 2002], zooplankton fecal pellets [*Gallinari et al.*, unpublished; *Schultes et al.*, 2004] and aggregates [*Moriceau et al.*, 2007] with data on $bSiO_2$ production, export and deep fluxes from 8 biogeochemical provinces of the world ocean [described in *Ragueneau et al.,* 2002]. The $bSiO_2$ downward fluxes are modeled to fit the downward flux data at the eight sites. This allows us to derive important information about particle formation in the upper ocean. The composition of the $bSiO_2$ fluxes in terms of large or small particles and, the sinking and specific $bSiO_2$ dissolution rates of each component help to unravel mechanisms involved in the spatial variability of the intensity and depth of $bSiO_2$ dissolution.

2. Approach: from laboratory experiments to a virtual water column

2.1. Experimental measurements

The flux of matter sinking through the water column is mainly composed of freely suspended phytoplankton cells, aggregates, and zooplankton fecal pellets [*Turner,* 2002; *Thornton,* 2002]. Specific $bSiO_2$ dissolution rates are usually measured experimentally on freely suspended diatoms [compiled by *Van Cappellen et al.,* 2002]. Recently, however, specific dissolution rates of $bSiO_2$ incorporated into aggregates [*Moriceau et al.*, 2007] and fecal pellets

78 [*Schultes*, 2004; *Gallinari*, unpublished] have been measured in the laboratory and shown to be
79 about half the rates measured on freely suspended diatoms (Table 1). Including the dissolution
80 rates of all particle types in models should enable us to predict the $bSiO_2$ sedimentation flux
81 more precisely. Here we consider a model of $bSiO_2$ flux with depth that includes two types of
82 particles (free diatom cells: FC and large particles: LP). We can keep the model simple with
83 only two particle types by assuming that the sinking rates and specific $bSiO_2$ dissolution rate of
84 aggregates and fecal pellets are similar as is demonstrated in Table 1. The FC group has the
85 slow sinking rate and fast specific $bSiO_2$ dissolution rate characteristic of free diatom cells. The
86 LP group has faster sinking rates than the FC and half the specific $bSiO_2$ dissolution rate. For
87 comparison, the model was first run using only one type of particle with sinking properties and
88 $bSiO_2$ dissolution rates between those of FC and LP particles as described below.
89 The data used for this study were collected in eight biogeochemical provinces of the
90 world ocean, for which annual measurements of $bSiO_2$ production, export and deep fluxes (at 2
91 depths) are available [data in *Ragueneau et al.*, 2002]. In this dataset, export fluxes (at 200 m)
92 were derived from models or from sediment trap measurements while deeper water fluxes (1000
93 and 3000 m depth) were measured using sediment traps. Two sites are located in the Equatorial
94 (EqPac) and North Pacific (OSP), and two in the North Atlantic Ocean (PAP and BATS). Four
95 are located in the Southern Ocean: one north of the Polar Front in the Pacific sector (NACC),
96 two in the Polar Front Zone of the Atlantic (APFA) and Pacific (APFP) sectors, and one just
97 south of the Polar Front in the Indian sector (POOZ) (see positions in Table 2). Four data points
98 can be fitted for each site, providing a total of 32 data points.
99

100 **2.2. Model description**

101 The concentration profiles of $bSiO_2$ for each particle pool i (LP or FC) can be described
102 by a simple advection-reaction model (Eq. 1):

$$\frac{\partial bSiO_{2i}}{\partial t} = -S_i \cdot \frac{\partial bSiO_{2i}}{\partial z} - k_i(T) \cdot bSiO_{2i} \quad (1)$$

where t is time (d), z depth (m), S_i is the sinking rate (m d^{-1}) , and $k_i(T)$ is the (temperature-dependent) first-order specific $bSiO_2$ dissolution rate (d^{-1}). Such first-order dissolution of $bSiO_2$ is often observed in batch experiments and leads to a simple exponential increase in the DSi concentration as a function of time [e.g. *Greenwood et al.*, 2001].

Assuming steady-state ($\frac{\partial bSiO_{2i}}{\partial t}$=0), and constant sinking and dissolution rates, the concentration (mmol m^{-3}) and flux of $bSiO_2$ (mmol m^{-2} d^{-1}) at each water column depth (z) are given by equation 2:

$$bSiO_{2i}(z) = bSiO_{2i}(0) \cdot e^{-\frac{k_i}{S_i} \cdot z} \quad (2)$$

which in terms of the total fluxes for the 1-particle model and the 2-particle model gives equation 3 and 3'respectively:

$$FbSiO_2(z) = PP_{bSiO2} \cdot e^{-\frac{k}{s} \cdot z} \quad (3)$$

$$FbSiO_2(z) = PP_{bSiO2} \cdot [\alpha \cdot e^{-\frac{k_{FC}}{S_{FC}} \cdot z} + (1-\alpha) \cdot e^{-\frac{k_{LP}}{s_{LP}} \cdot z}] \quad (3')$$

where α and (1- α) correspond to $bSiO_2$ production (PP_{bSiO2}, in mmol m^{-2} d^{-1}) in the FC and the LP groups in the upper layer, respectively.

As temperature is allowed to vary, we use a piecewise approximation to model equation 3. The water column is subdivided into a number of layers (with thickness Δz) in which temperature is assumed constant. Then, for each fraction, the flux at the bottom (z + Δz) and top (z) of this layer are related by:

$$FbSiO_{2i}(z+\Delta z) = FbSiO_{2i}(z)\cdot e^{-\frac{ki(T)}{S_i}\cdot\Delta z} \qquad (4)$$

For the 1-particle model the flux at z = 0 equals the $bSiO_2$ production (PP_{bSiO2}), and for the 2-particle model the $bSiO_2$ flux at each depth is the sum of the LP and FC fluxes.

$$\begin{aligned} FbSiO_{2FC}(0) &= \alpha\cdot PP_{bSiO2} \\ FbSiO_{2LP}(0) &= (1-\alpha)\cdot PP_{bSiO2} \\ FbSiO_{2TOT}(z) &= FbSiO_{2FC}(z) + FbSiO_{2LP}(z) \end{aligned} \qquad (5)$$

In these equations, $FbSiO_{2TOT}(z)$ is the flux of total $bSiO_2$ in mmol m^{-2} d^{-1} at depth z; PP_{bSiO2} is the production flux of $bSiO_2$ in mmol m^{-2} d^{-1}; $FbSiO_{2\ FC}(z)$ and $FbSiO_{2\ LP}(z)$ are the fluxes of $bSiO_2$ in the FC and LP groups at depth z respectively. $k_{FC}(T)$ and $k_{LP}(T)$ are the specific $bSiO_2$ dissolution rates in d^{-1} given in the literature for FC particles (Table 1) and corrected by the factor of 2 less that was measured experimentally for LP particles. Rates were also corrected for temperature, according to equation (6) from *Rickert et al.* [2002]; temperature profiles of the water column at each site were from the NODC (Levitus) World Ocean Atlas 1998 (*http://www.cdc.noaa.gov/).*

144 $$\ln(k_z(T_2)) = \ln(k_1) + \frac{E_{app}}{R} \times \left(\frac{1}{T_1} - \frac{1}{T_2} \right) \quad (6)$$

145

146 where k_1 is the specific $bSiO_2$ dissolution rate in d^{-1} measured in controlled conditions in the
147 laboratory; T_1 is the experimental temperature in degrees Kelvin (286.15 K); $k_z(T_2)$ is the rate
148 recalculated for the depth z at the in situ temperature T_2 ; and Eapp/R = 7211 °K.

149 To facilitate comparison among sites, the total flux is normalized to the production flux
150 to obtain a profile of $bSiO_2$ flux expressed in % of $bSiO_2$ production.

151 For both models we have:

152

153 $$\%FbSiO_2(z) = \frac{FbSiO_{2tot}(z)}{PP_{bSiO2}} \times 100 \quad (7)$$

154

155 which for the 2-particle model becomes:

156

157 $$\%FbSiO_2(z) = \frac{FbSiO_{2FC}(z) + FbSiO_{2LP}(z)}{PP_{bSiO2}} \times 100 \quad (7')$$

158

159 **2.3. Parameter determination**

160 As a first step, we applied the 1-pool model to fit the $bSiO_2$ flux profiles measured in the
161 field. The specific dissolution rate was set to the value given in Table 1 for FC, and corrected for
162 temperature at each site and depth using eq. 6. At each site, the model 1 calculated the $bSiO_2$
163 sinking rate required to fit the in situ $bSiO_2$ flux data. Note that the fit is not improved when the
164 model uses LP specific dissolution rates instead of k_{FC} nor an average of the two values.

In a second step, $bSiO_2$ specific dissolution rates and the sinking rates for two pools of particles were included in the model (model 2). Specific $bSiO_2$ dissolution rates of FC and LP were set to values presented in Table 1 and corrected for in situ temperature at each depth using equation 6. The model 2 calculated a global sinking rate for FC particles (S_{FC}) for all sites, one LP sinking rate per site and the percent of $bSiO_2$ from the production which is incorporated into large particles (1-α) or stays freely suspended (α).

Finally in a third step (model 3), the parameter S_{FC} was allowed to vary at each site.

In the three versions of the model, parameters were calculated by minimizing the sum of the square residuals using the Excel Solver and the GRG method (Generalized Reduced Gradient). These calculations were tested for many initial values because the algorithm used is non linear. Best fits to the data using the three model versions are shown for each of the eight sites in Fig. 1.

2.4. Statistical comparison of the 1-particle and 2-particle models

We used an F-test to compare the three versions of the model. The null hypothesis considers that adding complexity to the model does not significantly decrease the sum of the square residuals between model and observed data (SSR). The calculated F value is obtained using equation (8) and compared to the F test critical value.

$$F = (SSR1-SSR2)\ (df1-df2) / (SSR2/df2) \quad (8)$$

SSR1 and SSR2 are the sum of the square residuals between the modeled and the experimental values; df1 and df2 are the degrees of freedom of the different versions of the model calculated as follow.

$$dfi = E - P - 1 \quad (9)$$

With E, the number of observed values the models has to fit (4 data for each of the 8 sites), and P the number of variable parameters used to optimize the fit.

189 The F test was first applied to compare the 1-particle model (hereafter referred to as
190 model 1) to a 2-particle model using a global S_{FC} (model 2). Next, we compared two versions of
191 the 2-particle model, one using a global S_{FC} (model 2 again) and one using a variable S_{FC} at each
192 site (model 3). When the model considered only one type of particle, it had 23 degrees of
193 freedom. Model 2 used 17 parameters, providing14 degrees of freedom. Finally, model 3 had 7
194 degrees of freedom.

195

196 # 3. Results

197 ## 3.1. Comparison of the model versions: Importance of particle formation

198 Figure 1 shows the reconstructed $bSiO_2$ profiles at the eight sites for the three versions of
199 the model. Model 1 is clearly not able to fit the experimental data at any of the eight sites. When
200 the model uses two different pools of $bSiO_2$ but only one global S_{FC}, the $bSiO_2$ profiles are close
201 to the measured values except for APFP, NACC and PAP. The F-test determined, at a 99%
202 confidence level, that model 2 provides a better fit to the data than model 1. Thus the use of a
203 global S_{FC} of 2.76 m d^{-1} (Table 2) is a good approximation. Note that at the PAP site, the flux at
204 1000 m is low compared to the flux at 3000 m and can be explained by the presence of
205 swimmers in the trap [*Lampitt et al.,* 2001].

206 Model 2, which considered a global FC sinking rate (S_{FC}), gives more degrees of freedom
207 than model 1, but the use of a global S_{FC} is also an oversimplification. Indeed, for the PAP site in
208 the North East Atlantic Ocean, and for the NACC and APFP sites located in the Pacific sector of
209 the Southern Ocean (North of the Polar Front and on the Polar Front respectively), this approach
210 doesn't fit the data closely. To improve the reconstruction of these $bSiO_2$ fluxes, the model has
211 to use a S_{FC} higher than the global one. Reconstructions of the Southern Ocean profiles are
212 generally improved by using model 3 with a varying S_{FC} (Fig. 1). The F-test also favors model 3

over model 2 at the 95% confidence level. At the annual scale, FC sinking rates can be classified into two groups: fast S_{FC} in the Southern Ocean and PAP site and slow S_{FC} in the rest of the world. This trend may well reflect the production of large, fast sinking diatoms commonly observed in the Southern Ocean [*Kemp et al.,* 2006].

Freely suspended diatoms and large particles have such different sinking rates and specific $bSiO_2$ dissolution rates that parameters of the two groups of particles must be considered to correctly reconstruct $bSiO_2$ flux profiles. The role and importance of each particle type is confirmed by a sensitivity analysis performed on the profiles using model 3 for the sinking rates of the two particles (shown for POOZ, Fig. 2). Profiles of $bSiO_2$ fluxes are quite sensitive to variation in sinking rates: in the upper 1000 m the profile is mostly affected by the sinking rate of FC whereas deeper, the profile is more sensitive to variation of the LP sinking rate. The composition of the flux in the upper layer (parameter α) is well constrained, as when the contribution of FC and LP changes by only 5-10 %, the resulting profile of $bSiO_2$ flux significantly differs from the one measured (Fig. 2c).

3.2. Model outputs

For the eight sites, model 3 provides sinking rates ranging from 45 to 605 m d^{-1} for the LP and from 0.1 to 10.4 m d^{-1} for the FC (Table 2; Fig. 1), consistent with ranges found in the literature (Table 1). The sinking rates calculated by model 3 confirm the prevalence of aggregates and fecal pellets in the LP group (see values and references in Table1) and the fact that the FC group must be essentially composed of freely suspended diatoms, small and large. Note that the 2- particles models (models 2 and 3) can not always strictly separate LP and FC using $bSiO_2$ sinking and specific dissolution rates. For the two sites located in the Southern Ocean (APFP and NACC) and for PAP, model 3 produces faster FC sinking rates and a faster LP sinking rates than those calculated by model 2. The S_{FC} calculated by the model 2 is in these

cases lowered by the other sites' S_{FC}. The difference between the results of the two models for APFP, NACC and PAP shows the importance of a third group of particles that is included in LP in model 2 results and in FC in model 3 results. Large diatoms that have been observed in areas like the Southern Ocean, Gulf of California, and North Pacific Gyre [*Kemp et al.*, 2000, 2006] apparently dominate the production of APFP, NACC and PAP. Following the same argument, the very low S_{LP} and S_{FC} calculated by model 3 for APFA and POOZ suggest simultaneous production of small and large diatoms. Therefore, there are really three groups of particles (LP, freely-suspended large cells, and freely-suspended small cells); however, the large, freely-suspended diatoms have been included in the LP group here as the best compromise since the model can only account for two groups of particles.

Also, even if not shown here, giant aggregates with small and even null sinking rates such as those observed by *Rinaldi et al.* [1995] would certainly be integrated into the FC group of particles.

4. DISCUSSION

4.1. Particle formation: a major factor determining $bSiO_2$ export and recycling

In their global analysis of $bSiO_2$ production and dissolution, *Brzezinski et al.* [2003] demonstrated that the dissolution to production ratio integrated over the surface layer ($\int D:\int P$) is low under bloom conditions, leaving ample room for net export. They underlined the importance of considering dissolution when determining export of matter. Using the model results, we compare the importance of the two processes, sinking and dissolution, by calculating particle residence times in the mixed layer at each site with only sinking or only dissolution considered (Table 3). The comparison of these $bSiO_2$ residence times in surface waters suggests that this global data set of $bSiO_2$ production and dissolution cannot ignore particle formation. Sinking rates of large particles act on much shorter time scales than dissolution rates, so, rather than

263 having the export determined by the intensity of the recycling, the intensity of export (1-∫D:∫P) is
264 linked to the rate of large particle formation and drives the intensity of shallow-water recycling.
265 The rate at which diatoms are incorporated into large particles will determine how rapidly
266 exported they are as their fast sinking rates leave no time for dissolution to occur in surface
267 waters. In such cases, the dissolution depth is translated downward. The recycling intensity in
268 surface waters depends first on the ability of diatoms to remain as single cells and secondly on
269 factors such as temperature [*Bidle et al.*, 2002; *Fujii and Chai*, 2005; *Lawson et al.*, 1978] and
270 bacterial activity [*Bidle and Azam*, 1999] which control their fate in surface waters.

271 Thus, we suggest that low ∫D:∫P ratios under bloom conditions [*Brzezinski et al.*, 2003]
272 are caused by a rapid export of bloom diatoms [*Buesseler*, 1998], which extracts $bSiO_2$ from the
273 surface waters where intense recycling generally occurs under non-bloom conditions.
274 Recognizing the importance of seasonality to the sinking of particles, we calculated the
275 seasonality index of each site as defined by *Berger and Wefer* [1990] (Table 2) as six minus the
276 number of months necessary to generate one half of the annual productivity when the data are
277 ordered from the most productive to the least productive month (the 'production half-time').
278 Considering productivity, the eight sites could be classified in three groups [*Berger and Wefer*,
279 1990]: EqPac and BATS have constant productivity (seasonality index close to 0); OSP, APFA,
280 NACC, POOZ, PAP have sinusoidal production (seasonality index between 2 and 3) and APFP
281 has a strong seasonal peak in productivity (seasonality index > 3.5). As shown in Figure 3, sites
282 exhibiting the lowest seasonality (EqPac, BATS) also exhibit the lowest export at 100 m (i.e. low
283 1-∫D:∫P). Conversely, sites with higher seasonality (APFP, NACC and APFA) display a larger 1-
284 ∫D:∫P at 100 m. Even if seasonality is not the only important factor, Figure 3 confirms its major
285 role in particle formation. Indeed grazing and aggregation processes are more abundant at the
286 end of a bloom [*Buesseler,* 1998] and consequently the export of matter out of the surface layer
287 is also increased. To properly model diatom export versus recycling, further research efforts

must focus not only on dissolution properties, but perhaps more importantly, on representing particle formation during bloom termination.

Another implication of our model results concerns the ballast theory. *Armstrong et al.* [2002] established a correlation between organic carbon and ballast ($bSiO_2$, $CaCO_3$) fluxes below the mixing layer. Based on this model, *Klaas and Archer* [2002] concluded that organic carbon is carried into the deeper waters preferentially by calcium carbonate, which has a higher density (2.71 g cm^{-3}) than opal (2.1 g cm^{-3}). *Passow* [2004] proposed the inverse of this hypothesis, that carbon, in the form of TEP, could transport organic matter and ballast to the deep sea by promoting aggregation. In APFP, OSP and NACC sites (Table 2), the fast S_{LP} suggested the dominance of large diatoms. At these sites, freely suspended diatoms can be exported from the mixed layer (Table 4) due to the low temperature at the surface layer and/or high sinking rates. But at most other sites, even ballasted with a frustule whose density is twice that of organic matter (1.06 g cm^{-3}), a single diatom almost completely dissolves in the upper WML. This observation calls for more caution when considering the ballast theory and emphasizes once again the importance of bloom-ending processes to explain sedimentation fluxes. The fact that POC and ballast fluxes are closely linked below the mixed layer [*Armstrong et al.,* 2002] is not necessarily related only to the higher density of $bSiO_2$ and $CaCO_3$ compared to that of organic matter. The efficiency of sedimentation depends primarily on the incorporation of diatoms into large particles like aggregates or fecal pellets (Fig. 2c) in the mixed layer; the ballasting of these large particles throughout the whole water column plays a secondary role (Fig. 2b).

4.2. Implications for the silicate pump

The silicate pump is the process by which $bSiO_2$ is exported from surface waters with a greater efficiency than PON, driving the system towards DSi limitation. According to *Dugdale et*

313 *al.*, [1995], grazers are the motor of this silicate pump; whereas nitrogen is largely assimilated or
314 recycled by grazers and therefore retained at the surface, $bSiO_2$ is packaged into fast-sinking
315 fecal pellets and exported from the mixed layer. The silicate pump model was developed initially
316 for the Equatorial Pacific [*Dugdale and Wilkerson*, 1998] and later applied to the Southern
317 Ocean [*Brzezinski et al.*, 2001]. It is based on several assumptions, including that $bSiO_2$
318 dissolution in surface waters is negligible [*Dugdale et al.*, 1995]. Our results clearly contradict
319 this assumption at the EqPac site [*Dugdale and Wilkerson,* 1998]. EqPac is the site with the
320 shallowest recycling in our model output (Fig. 1), as observed previously in the field [*Blain et*
321 *al.*, 1999]. The EqPac site is well-known for its low export efficiency [*Buesseler*, 1998], possibly
322 related to its small seasonal variability (Table 2, Fig. 3). Consequently, the fraction of $bSiO_2$
323 production incorporated into large particles by aggregation/ fecal pellet production is lowest at
324 the EqPac site on an annual basis (Table 2). Our results (Table 4) suggest that the vast majority
325 of the diatoms remain as single cells in surface waters, and 88% dissolve before reaching the
326 base of the mixed layer (on average, 50 m). This extensive dissolution is consistent with the high
327 temperatures (i.e., high dissolution rate) and bacterial activity (i.e., fast removal of protective
328 organic coatings) encountered in these equatorial waters [*Bidle et al.*, 2002]. It is important to
329 note that these are annual fluxes. Episodic events such as Tropical Instability Waves have been
330 shown to trigger intense diatom concentrations at fronts [*Yoder et al.,* 1994], leading to massive
331 sinking of algal material and the formation of large flocs of phytodetritus on the seafloor [*Smith*
332 *et al.,* 1996]. However, although these episodes may be very important for sustaining life in the
333 mesopelagic and at the sediment-water interface [*Smith et al.,* 2002; *Smith Jr et al.,* 2002], or for
334 formation of paleoceanographic records [*Ragueneau et al.*, 2000], our results suggest that they
335 do not contribute appreciably to annual POC and $bSiO_2$ fluxes in oligotrophic ecosystems.

336 *Brzezinski et al*. [2003] have suggested that a measure of the strength of the silicate pump
337 can be obtained by comparing $1-\int D:\int P$ for Si with the f-ratio for N (representing export intensity
338 for Si and N respectively). When the $1-\int D:\int P$ values obtained from our model are plotted versus

339 the f-ratio for each site (obtained from *Nelson et al.* [2002] for the Southern Ocean and from
340 *Falkowski et al.* [2003] for the other sites) (Fig. 4), the silica pump appears to be most
341 pronounced at APFP and NACC sites. At the EqPac site, 1-∫D:∫P is close to 0.12, whereas the f-
342 ratio is between 0.1 and 0.17 [*Dugdale et al.*, 1992; *Mc Carthy et al.*, 1996]. Since 1-∫D:∫P is less
343 than or equal to the f-ratio at this site, it would appear that the silicate pump is weak or
344 nonexistent.

345 The silicate pump will be most pronounced under the following two conditions: (1) when
346 particle formation is extensive enough to induce rapid export from the mixed layer, and (2) when
347 Si and N cycling are decoupled, so that more Si is exported relative to N. To simplify the model
348 as much as possible, we pooled aggregates and fecal pellets into a single group to reconstruct
349 $bSiO_2$ fluxes. This simplification may lead to some inaccuracies, as grazing (i.e., fecal pellet
350 production) and aggregation can have very different effects on the silicate pump [see *Ragueneau*
351 *et al.*, 2006]. While grazers assimilate C and N from diatom material, $bSiO_2$ passes through the
352 gut quasi-inertly, leading to a five-fold increase in the Si/C ratio as the material is egested
353 [*Cowie and Hedges*, 1996; *Tande and Slagstad*, 1985]. By contrast, diatoms that are incorporated
354 within aggregates rather than ingested by zooplankton would tend to remain alive for a longer
355 time, fixing their Si/C ratio at a relatively constant value [*Moriceau et al.*, 2007]. Despite this
356 caveat, with our simple model we can at least identify sites with a high flux of fast-sinking
357 particles, and see that 1-∫D:∫P (at 100 m) is highest at sites with the most seasonality (Fig. 3).
358 Clearly, particle formation at the end of blooms is a key factor controlling the silicate pump.
359 Further investigation of aggregation dynamics is crucial for understanding temporal and spatial
360 variations in the strength of the silicate pump, as well as the role of diatoms in the biological
361 carbon pump [e.g., *Ragueneau et al.*, 2006].

362

363 **4.3. Impact on the geochemistry of the seafloor**

Our results have important implications for the calibration of $bSiO_2$ mass accumulation rates (MAR) as a proxy of paleoproductivity [*Ragueneau et al.*, 2000]. Larger opal MAR need not necessarily be ascribed to higher surface productivity. At the POOZ site (Fig. 2), for example, a doubling in the $bSiO_2$ rain rate can be achieved without any change in surface $bSiO_2$ production, through either (1) a doubling in the incorporation of $bSiO_2$ into large particles (i.e., from 20% to 40%), (2) a 3.33-fold increase in the LP sinking rate (from 30 to 100 m d^{-1}), or (3) a 2.67-fold decrease in the LP dissolution rate from 0.04 to 0.015 d^{-1}. These ranges in values are all realistic, and a small variation in one of them can significantly increase the amount of $bSiO_2$ reaching the seafloor. Furthermore, these 3 factors are not necessarily independent and can therefore have additive effects. For example, incorporation into large particles would most likely increase both the particle sinking rate and decrease the $bSiO_2$ dissolution rate [*Moriceau et al.*, 2007]. Clearly, improving our understanding of how siliceous sediments accumulate requires proper consideration of particle formation and biogeochemical cycling in sinking particles. This is crucial not only for determining the depth of $bSiO_2$ dissolution in the water column, but also the extent of silica burial in sediments [*Gallinari et al.*, 2002; *Khalil et al.*, 2007].

5. Conclusions and perspectives

In this paper, we have combined sinking and silica dissolution rates [*Schultes*, 2004; *Moriceau et al.,* 2007] for three types of siliceous particles (diatoms as free cells, incorporated into zooplankton fecal pellets, or into aggregates) to reconstruct theoretical downward profiles of $bSiO_2$ fluxes. By applying a simple advection-reaction model to 8 sites of the world ocean where annual estimates of $bSiO_2$ production are available [*Ragueneau et al.,* 2002], we were able to fit these theoretical profiles to measured $bSiO_2$ fluxes derived from sediment trap data. Such an approach allowed us to derive the sinking rates of particles and partitioning of $bSiO_2$ between freely-suspended diatoms and large particles. When diatoms are incorporated into large particles

389 via aggregation or incorporation into fecal pellets, this can impact $bSiO_2$ recycling and possibly
390 other elements like C and N. Further experimentation would be needed, however, to assess this
391 last point.

392 The competition between recycling in surface waters and export to depth is controlled by
393 the intensity of particle formation rather than by the extent of dissolution in surface waters. For
394 $bSiO_2$ incorporated into sinking aggregates and fecal pellets, export is much faster than
395 dissolution. Therefore, the extent of dissolution in surface waters depends primarily on the
396 amount of diatom cells that remain freely suspended and can subsequently be degraded by
397 bacteria [*Bidle and Azam*, 1999]. Thus, even ballasted by its frustule, a diatom would be recycled
398 if not incorporated into fast-sinking aggregates or fecal pellets.

399 This finding also has implications for the use of opal MAR as a proxy of
400 paleoproductivity, which should account not only for the production signal, but also the extent of
401 incorporation into large particles. Furthermore, just as $bSiO_2$ preservation depends on the types
402 of particles transporting diatoms toward the seafloor, it likely affects C preservation as well.
403 Further investigation is needed of the extent of C recycling within aggregates and fecal pellets, as
404 this has major implications for C export and benthic food webs.

405 Our model demonstrated that dissolution in surface waters is extremely high at the EqPac
406 site, most likely due to the small percentage of $bSiO_2$ production being incorporated, on an
407 annual basis, into large sinking particles (Table 2). This result does not support the idea of a
408 strong silicate pump in the equatorial Pacific, as previously suggested by *Dugdale et al*. [1995].
409 Rather, it appears that such a mechanism would be most applicable at highly seasonal sites like
410 NACC or APFP where the fraction of $bSiO_2$ production that is exported from the surface layer is
411 highest (Fig. 3). At such locations, the efficiency of the silica pump will depend upon the relative
412 fates of Si and N in sinking particles. Since aggregation and incorporation into fecal pellets may
413 have very distinct influences on Si and N decoupling during sinking [*Ragueneau et al*., 2006],
414 differentiating between these two transport pathways is essential for improving our

415 understanding of the functioning of the silicate pump, the role of diatoms in the biological pump,
416 and the nutritional properties of particles supporting deep-sea food webs.
417
418
419
420
421
422
423

Acknowledgements. We are grateful to Monique Briand for her technical assistance with graphics. Thanks to Sorcha Ni Longphuirt, Cindy Lee and Lynn Abramson who kindly commented on this paper and corrected it from the English mistakes. The authors acknowledge NODC (Levitus) World Ocean Atlas 1998 for their data provided by the NOAA-CIRES Climate Diagnostics Center, Boulder, Colorado, USA, from their Web site at http://www.cdc.noaa.gov/. This work has been funded by the EU which is greatly acknowledged, partly through the ORFOIS (EVK2-CT2001-00100) project and partly through the Si-WEBS (HPRN-CT-2002-00218) Research Training network of the Marie Curie program. This is contribution # xxx of the IUEM.

434 References

435 Alldredge, A. L. and C. Gotschalk (1988), In situ settling behaviour of marine snow, *Limnol*
436 *Oceanogr, 33* (3), 339-351.
437 Armstrong, R. A., C. Lee, J. I. Hedges, S. Honjo and S. G. Wakeham (2002), A new,
438 mechanistic model for organic carbon fluxes in the ocean based on the quantitative association of
439 POC with ballast minerals, *Deep-Sea Res Part II, 49*, 219-236.
440 Aumont, O., E. Maier-Reimer, S. Blain and P. Monfrey (2003), An ecosystem model of the
441 global ocean including Fe, Si, P colimitations, *Global Biogeochem Cycles, 17*, 1-26.
442 Berger, W. H. and G. Wefer (1990), Export production: seasonality and intermittency, and
443 paleoceanographic implications, *Palaeogeogr Palaeoclimatol Palaeoecol, 89*, 245-254.
444 Bidle, K. D. and F. Azam (1999), Accelerated dissolution of diatom silica by marine bacterial
445 assemblages, *Nature, 397*, 508-512.
446 Bidle, K. D., M. Manganelli and F. Azam (2002), Regulation of Oceanic Silicon and Carbon
447 Preservation by Temperature Control on bacteria, *Science, 298*, 1980-1984.
448 Bienfang, P. K. (1981), Sinking rate of heterogeneous, temperate phytoplankton populations, *J*
449 *Plankton Res, 3* (2), 235-253.
450 Blain, S., P. Tréguer and M. Rodier (1999), Stocks and fluxes of biogenic silica in the western
451 oligotrophic equatorial Pacific, *J Geophys Res, 104*, 3357-3367.
452 Brzezinski, M. A., D. M. Nelson, V. M. Franck and D. E. Sigmon (2001), Silicon dynamics
453 within an intense open-ocean diatom bloom in the Pacific Sector of the Southern Ocean, *Deep-*
454 *Sea Res, 48*, 3997-4018.
455 Brzezinski, M. A., J. L. Jones, K. D. Bidle and F. Azam (2003), The balance between silica
456 production and silica dissolution in the sea: Insights from Monterey Bay, California, applied to
457 the global data set, *Limnol Oceanogr, 48* (5), 1846-1854.
458 Buesseler, K. O. (1998), The decoupling of production and particulate export in the surface
459 ocean, *Global Biogeochem Cycles, 12*, 297-310.

460 Cowie, G. L. and J. I. Hedges (1996), Digestion and alteration of the biochemical constituents of
461 a diatom (*Thalassiosira weissflogii*) ingested by an herbivorious copepod (*Calanus pacificus*),
462 *Limnol Oceanogr, 41*, 581-594.
463 Cushing, D. H. (1989), A difference in structure between ecosystems in strongly stratified waters
464 and in those that are only weakly stratified, *J Plankton Res, 11*, 1-13.
465 Dugdale, R. C., F. P. Wilkerson, R. T. Barber and F. P. Chavez (1992), Estimating new
466 production in the equatorial Pacific Ocean at 150°W, *J Geophys Res, 97* (C1), 681-686.
467 Dugdale, R. C., F. P. Wilkerson and H. J. Minas (1995), The role of a silicate pump in driving
468 new production, *Deep-Sea Res Part I, 42*, 697-719.
469 Dugdale, R. C. and F. P. Wilkerson (1998), Silicate regulation of new production in the
470 equatorial Pacific upwelling, *Nature, 391*, 270-273.
471 Falkowski, P. G., E. A. Laws, R. T. Barber, and J. W. Murray (2003), Phytoplankton and their
472 role in primary, new and export production, in *Ocean Biogeochemistry,* edited by M. J. R.
473 Fasham, Berlin, Springer-Verlag.
474 Fujii, M. and F. Chai (2005), Effects of biogenic silica dissolution on silicon cycling and export
475 production, *Geophys Res Lett, 32*, L05617. doi: 10.1029/2004GL02054.
476 Gallinari, M., O. Ragueneau, L. Corrin, D. J. Demaster, and P. Tréguer (2002) The importance
477 of water column processes on the dissolution properties of biogenic silica in deep sea-sediments
478 I. Solubility, *Geochim Cosmochim Acta, 66***,** 2701-2717.
479 Greenwood, J., V. W. Truesdale and A. R. Rendell (2001), Biogenic silica dissolution in
480 seawater - in vitro chemical kinetics, *Prog Oceanogr, 48*, 1-23.
481 Kemp A. E. S., J. Pike, R. B. Pearce, and C. B. Lange (2000), The "Fall dump" - a new
482 perspective on the role of a "shade flora" in the annual cycle of diatom production and export
483 flux, *Deep-Sea Res Part I, 47,* 2129-2154.
484 Kemp, A. E. S., R. B. Pearce, I. Grigorov, J. Rance, C. B. Lange, P. Quilty, and I. Salter (2006),
485 The production of giant marine diatoms and their export at oceanic frontal zones: implications

for Si and C flux in stratified oceans, *Global Biogeochem Cycles, 20*. doi:10.1029/2006GB002698.

Khalil, K., C. Rabouille, M. Gallinari, and O. Ragueneau (2007), Constraining biogenic silica dissolution in marine sediments: a comparison between diagenetic models and experimental dissolution rates, *Mar Chem,* in press. doi:10.1016/j.marchem.2006.12.004.

Klaas, C. and D. E. Archer (2002), Association of sinking organic matter with various types of mineral ballast in the deep sea: Implications for the rain ratio, *Global Biogeochem Cycles, 16* (4), 116, doi:10.1029/2001GB001765.

Lampitt, R. S., K. Kiriakoulakis, O. Ragueneau, A. Vangriesheim and G. Wolff (2001), Material supply to the abyssal seafloor in the Northeast Atlantic, *Prog Oceanogr, 50* (1-4), 27-63.

Lawson, S. D., D. C. Hurd and H. Stuart Pankratz (1978), Silica dissolution rates of decomposing phytoplankton assemblages at various temperature, *Am J Sci, 278*, 1373-1393.

Leynaert, A., P. Tréguer, C. Lancelot and M. Rodier (2001), Silicon limitation of biogenic silica production in the Equatorial Pacific, *Deep-Sea Res Part I, 48*, 639-660.

Mann, K. H. and J. R. N. Lazier (Eds) (1996), *Dynamics of Marine Ecosystems: Biological-Physical Interactions in the Oceans*, 394 pp., Blackwell Science.

McCarthy, J. J., C. Garside, J. L. Nevins, R. T. Barber and J. W. Murray (1996), New production along the 140°W in the equatorial Pacific during and following the 1992 El Nino event, *Deep-Sea Res Part II, 43* (4-6), 1065-1093.

Moriceau, B., M. Garvey, U. Passow and O. Ragueneau (2007), Evidence for reduced biogenic silica dissolution rates in diatom aggregates, *Mar Ecol Prog Ser, 333,* 129-142.

Nelson, D. M., P. Tréguer, M. A. Brzezinski, A. Leynaert and B. Quéguiner (1995), Production and dissolution of biogenic silica in the ocean: Revised global estimates, comparison with regional data and relationship to biogenic sedimentation, *Global Biogeochem Cycles, 9* (3), 359-372.

511 Nelson, D. M., R. F. Anderson, R. T. Barber, M. A. Brzezinski, K. Buesseler, Z. Chase, R. W.
512 Collier, M. -L. Dickson, R. François, M. R. Hiscock, S. Honjo, J. Marra, W. R. Martin, R. N.
513 Sambrotto, F. L. Sayles, and D. E. Sigmon (2002), Vertical budgets for organic carbon and
514 biogenic silica in the pacific sector of the Southern Ocean, 1996-1998, *Deep-Sea Res II, 49***,**
515 1645-1674.
516 Officer, C. B. and J. H. Ryther (1980), The possible importance of silicon in marine
517 eutrophication, *Mar Ecol Prog Ser, 3*, 83-91.
518 Passow, U. (2004), Switching perspectives: Do mineral fluxes determine particulate organic
519 carbon fluxes or vice versa? *Geochemistry Geophysics Geosystems, 5* (4), 1-5.
520 doi:10.1029/2003GC000670.
521 Pondaven, P., C. Fravalo, D. Ruiz-Pino, P. Tréguer, B. Quéguiner and C. Jeandel (1998),
522 Modelling the silica pump in the Permanently Open Ocean Zone of the Southern Ocean, *J Mar*
523 *Syst, 17*, 587-619.
524 Ragueneau, O., P. Tréguer, A. Leynaert, R. F. Anderson, M. A. Brzezinski, D. J. Demaster, R. C.
525 Dugdale, J. Dymond, G. Fischer, R. François, C. Heinze, E. Maier-Reimer, V. Martin-Jézéquel,
526 D. M. Nelson and B. Quéguiner (2000), A review of the Si cycle in the modern ocean: recent
527 progress and missing gaps in the application of biogenic opal as a paleoproductivity proxy,
528 *Global Planet Change, 26*, 317-365.
529 Ragueneau, O., N. Dittert, P. Pondaven, P. Tréguer and L. Corrin (2002), Si/C decoupling in the
530 world ocean: is the Southern Ocean different? *Deep-Sea Res Part II, 49*, 3127-3154.
531 Ragueneau, O., S. Schultes, K. Bidle, P. Claquin, et B. Moriceau, (2006), Si and C interactions
532 in the world ocean: importance of ecological processes and implications for the role of diatoms
533 in the biological pump, *Global Biogeochem Cycles, 20*, doi:1029/2006GB002688.
534 Rickert, D., M. Schlüter and K. Wallmann (2002), Dissolution Kinetics of biogenic silica from
535 the water column to the sediments, *Geochim Cosmochim Acta, 66* (3), 439-455.

536 Ridgwell, A. J., A. J. Watson and D. E. Archer (2002), Modeling the response on the oceanic Si
537 inventory to perturbation, and consequences for atmospheric CO2, *Global Biogeochem Cycles, 16* (4), 1071.
539 Rinaldi, A., R. A. Vollenweider, G. Montanari, C. R. Ferrari and A. Ghetti (1995), Mucilages in
540 italian seas: the Adriatic and Thyrrhenian Seas, 1988-1991, *The Science of the Total*
541 *Environment, 165*, 165-183.
542 Sarmiento, J. L., J. Dunne and R. A. Armstrong (2004), Do We Now Understand The Ocean's
543 Biological Pump? *U.S. JGOFS Newsletter, 12* (4), 1-5.
544 Schultes, S. (2004), The role of mesozooplankton grazing in the biogeochemical cycle of silicon
545 in the Southern Ocean, Ph. D., 168 pp., Universität Bremen, Bremen.
546 Smayda, T. J. (1970), The sinking and suspension of phytoplankton in the sea, *Oceanogr Mar*
547 *Biol Annu Rev, 8*, 353-414.
548 Smetacek, V. (1999), Diatoms and the Ocean Carbon Cycle, *Protist, 150*, 25-32.
549 Smith, C. R., D. J. Hoover, S. E. Doan, R. H. Pope, D. J. Demaster, F. C. Dobbs and M. A.
550 Altabet (1996), Phytodetritus at the abyssal seafloor across 10° of latitude in the central
551 equatorial Pacific, *Deep-Sea Res Part II, 43*, 1309-1338.
552 Smith, C. R., S. L. Minks, A. G. Glover, D. J. Demaster and P. Y. Sumida (2002),
553 FOODBANCS on the Antarctic Peninsula Shelf: the benthic food bank hypothesis and the
554 seasonal deposition pulse., *EOS Trans Am Geophys Union, 83* (4), 223.
555 Smith Jr, K. L., R. J. Baldwin, D. M. Karl and A. Boetius (2002), Benthic community responses
556 to pulses in pelagic food supply: North Pacific subtropical Gyre, *Deep-Sea Res Part I, 49*, 971-
557 990.
558 Tande, K. S. and D. Slagstad (1985), Assimilation efficiency in herbivorous aquatic organisms-
559 the potential of the ratio method using ^{14}C and biogenic silica as markers, *Limnol Oceanogr, 30*,
560 1093-1090.

561 Thornton, D. C. O. (2002), Diatom aggregation in the sea: mechanisms and ecological
562 implications, *Eur J Phycol, 37*, 149-161.
563 Tréguer, P., D. M. Nelson, A. J. V. Bennekom, D. J. Demaster, A. Leynaert and B. Quéguiner
564 (1995), The silica Balance in the World Ocean: A Reestimate, *Science, 268*, 375-379.
565 Turner, J. T. (2002), Zooplankton faecal pellets, marine snow and sinking phytoplankton
566 blooms, *Aquat Microb Ecol, 27*, 57-102.
567 Van Cappellen, P., S. Dixit and J. Van Beusekom (2002), Biogenic silica dissolution in the
568 oceans: Reconciling experimental and field-based dissolution rates, *Global Biogeochem Cycles,*
569 *16* (4), 1075, doi:10.1029/2001 GB001431.
570 Wassmann, P., L. Hansen, I. J. Andreassen, C. W. Riser and J. Urban-Rich (1999), Distribution
571 and sedimentation of faecal pellets on the Nordvestbanken shelf, northern Norway, in 1994,
572 *Sarsia, 84*, 239-252.
573 Yoder, J. A., S. G. Ackelson, R. T. Barber, P. Flamant, and W. M. Balch (1994), A line in the
574 sea, *Nature, 371***,** 689-692.

Figure caption

Figure 1: Best fits (lines) of the three versions of the models and in situ (dots) $bSiO_2$ flux profiles, for eight sites in the global ocean described in *Ragueneau et al.* [2002] (positions given in Table 2). The dashed lines are the fits obtained from the 1-particle model, the dotted lines describe the $bSiO_2$ fluxes calculated with the 2-particle model that uses a global S_{FC} and the plain lines depict the $bSiO_2$ profiles obtained from the 2-particle model that uses a variable S_{FC} calculated at each site.

Figure 2: Sensitivity of the model, represented by successive variation of parameters. Fig. 2a sensitivity of the model to the sinking rate of the slow sinking/fast dissolving particle S_{FC}, with S_{LP} set at 51 m d^{-1} and α at 68%, Fig. 2b, sensitivity of the model to the sinking rate of the fast sinking/slow dissolving particle S_{LP}, with S_{FC} set at 1.4 m d^{-1} and α at 68%, Fig. 2c, sensitivity of the model to the repartition of the $bSiO_2$ between the FC group α, and the LP group (1- α), with S_{LP} set at 51 m d^{-1} and S_{FC} at 1.4 m d^{-1}. The graphs represent the results of the test for the POOZ site, the full circles and the full lines in each graph represent the in situ measurements of the $bSiO_2$ fluxes and the results of the model 3.

Figure 3: Importance of the seasonality. 1-$\int$D:$\int$P at 100 m calculated from the model outputs as a function of the seasonality index [*Berger and Wefer* 1990]. The site names are given near each corresponding point.

Figure 4: 1-$\int$D:$\int$P calculated at 100 m with the model 3 versus the f-ratios. The f-ratios are from *Nelson et al.* [2002] for the Southern Ocean and *Falkowski et al.* [2003] for the other sites. The names of seven of the eight sites are indicated near the corresponding point. APFA site is not in the graph as no f-ratio is available at this site. The plain line delimits the zones where f-ratio is higher or lower than 1-$\int$D:$\int$P at 100 m which gives an indication of the strength of the silica pump.

	sinking rate m d^{-1}		dissolution rate d^{-1}		
	range	**References**	**range**	**References**	**Used in this study**
Cells	0.2-20	*Bienfang*, 1981; *Mann and Lazier*, 1996; *Smayda*, 1970; *Turner*, 2002]	0.005-1.3	[*Van Cappellen et al.*, 2002]	0.044
Aggregates	1-370	[*Alldredge and Gotschalk*, 1988; *Ridgwell et al.*, 2002]	0.012-0.056	[*Moriceau et al.*, 2007]	0.022
Copepod fecal pellets	5-220	[*Turner*, 2002; *Wassmann et al.*, 1999]	0.003-0.027	[*Gallinari et al.*,unpubl.; *Schultes,* 2004]	

Table 1: Range of sinking rates and specific dissolution rates cited in the literature for freely suspended cells, aggregates and copepods fecal pellets. The column "Used in this study", gives the dissolution values actually used herein. For the slow sinking/fast dissolving group (FC), we used the mean value given by *Van Cappellen et al.* [2002] from a compilation of studies, whereas for the LP (aggregates + fecal pellets) the rates are calculated from the average value given by *Van Cappellen et al.* [2002] divided by the factor of two which is the average decrease in dissolution rates observed when cells are incorporated into fecal pellets and aggregates [*Gallinari et al.*, unpubl; *Schultes*, 2004; *Moriceau et al.*, 2007].

		POOZ	APFP	NACC	APFA	OSP	EqPac	BATS	PAP
Latitude		-52	-60	-56.9	-50.1	50	1	28	48.8
Longitude		62	-170	-170.1	5.8	-145	-139	-67.5	-16.5
MMLD (m)		259	235	390	180	100	48	100	576
SI		2.80	3.75	2.80	2.70	2.50	0.33	1.30	3.00
Model 2: 2-particle model global S_{FC}	**% PP_{bSiO2} in FC stage α**	80%	70%	40%	20%	69%	88%	83%	65%
	S_{FC} (m d^{-1})				2.76				
	% PP_{bSiO2} into LP (1- α)	20%	30%	60%	80%	31%	12%	17%	35%
	S_{LP} (m d^{-1})	470	53	27	47	90	812	92	55
Model 3: 2-particle model variable S_{FC}	**% PP_{bSiO2} in FC stage α**	68%	81%	78%	17%	64%	88%	83%	85%
	S_{FC} (m d^{-1})	1.4	4.5	10.3	0.1	2	0.1	0.1	6.7
	% PP_{bSiO2} into LP (1- α)	32%	19%	22%	83%	36%	12%	17%	15%
	S_{LP} (m d^{-1})	51	452	242	45	62	500	90	605

Table 2: Environmental characteristics and results of the two versions of the 2-particle model calculated to fit the $bSiO_2$ flux profiles at eight sites of the global ocean (Fig. 1). The depth of the maximum mixed layer (MMLD) and the location of the sites are from *Ragueneau et al.* [2002]. The seasonality indexes (SI) are calculated following the work of *Berger and Wefer* [1990]. The last rows depict combinations of sinking rates for FC (S_{FC}) and LP (S_{LP}) and percentage of $bSiO_2$ incorporated into the two groups of particles calculated with each version of the 2-particle model from the best fits.

		POOZ	APFP	NACC	APFA	OSP	EqPac	BATS	PAP
residence time of FC in surface layer	**Considering only sinking**	0.7	0.2	0.1	10	0.5	10	10	0.15
	Considering dissolution	56	56	43	60	36	8	8	21
residence time of LP in surface layer	**Considering only sinking**	0.020	0.002	0.004	0.022	0.016	0.002	0.011	0.002
	Considering dissolution	113	113	86	121	71	15	17	42

Table 3: Residence times of the particles in the mixing layer (ML) in days calculated considering only dissolution processes and considering only sedimentation rates at the eight sites. To calculate the residence time of the particles considering only sinking processes, the sinking rates are normalized by the depth of the mixed layer (MLD) as given Table 2. The residence times of the particles in the mixed layer considering only dissolution processes are equal to 1/ k(T), with k(T) the specific dissolution rates corrected for temperature at each site.

	POOZ	APFP	NACC	APFA	OSP	EqPac	BATS	PAP
% PP_{bSiO2} reaching the MMLD	34%	53%	58%	80%	50%	12%	16%	18%
% PP_{bSiO2} on FC stage at the MMLD	4%	34%	36%	0%	16%	0%	0%	3%
% PP_{bSiO2} reaching the seafloor	17%	18%	18%	37%	19%	11%	7%	14%

Table 4: $bSiO_2$ fluxes of the eight sites at the maximum mixed layer depth (MMLD) (see also Table 2), in terms of % of total $bSiO_2$ production at the surface layer (PP_{bSiO2}), contribution of the slow sinking/fast dissolving group (FC) to the % of PP_{bSiO2} that reaches this depth, and % of PP_{bSiO2} that sinks down to the seafloor.

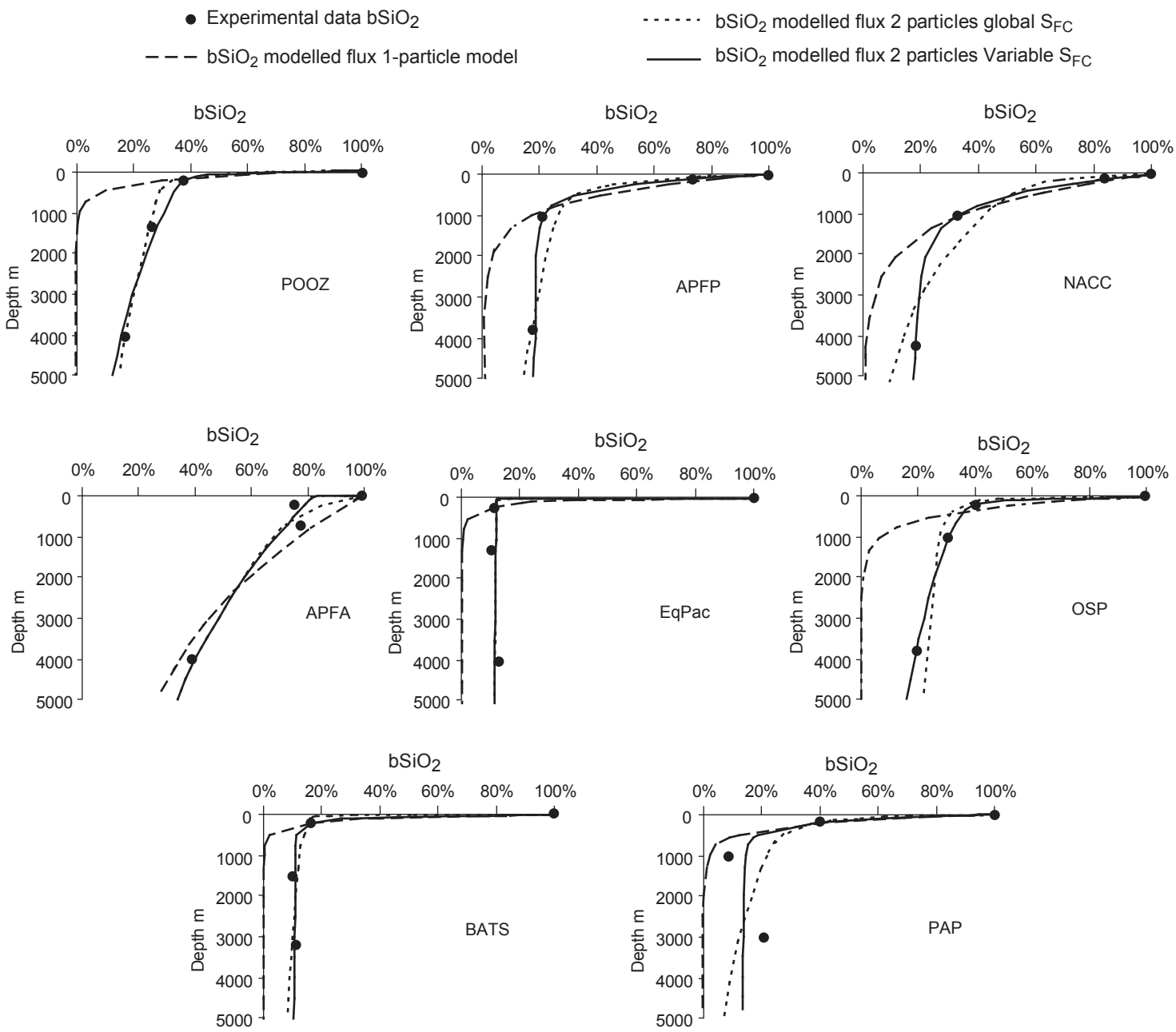
Experimental data bSiO2
bSiO2 modelled flux 1-particle model
bSiO2 modelled flux 2 particles global SFC
bSiO2 modelled flux 2 particles Variable SFC
bSiO2
0% 20% 40% 60% 80% 100%
0 1000 2000 3000 4000 5000
Depth m
POOZ
APFP
NACC
APFA
EqPac
OSP
BATS
PAP

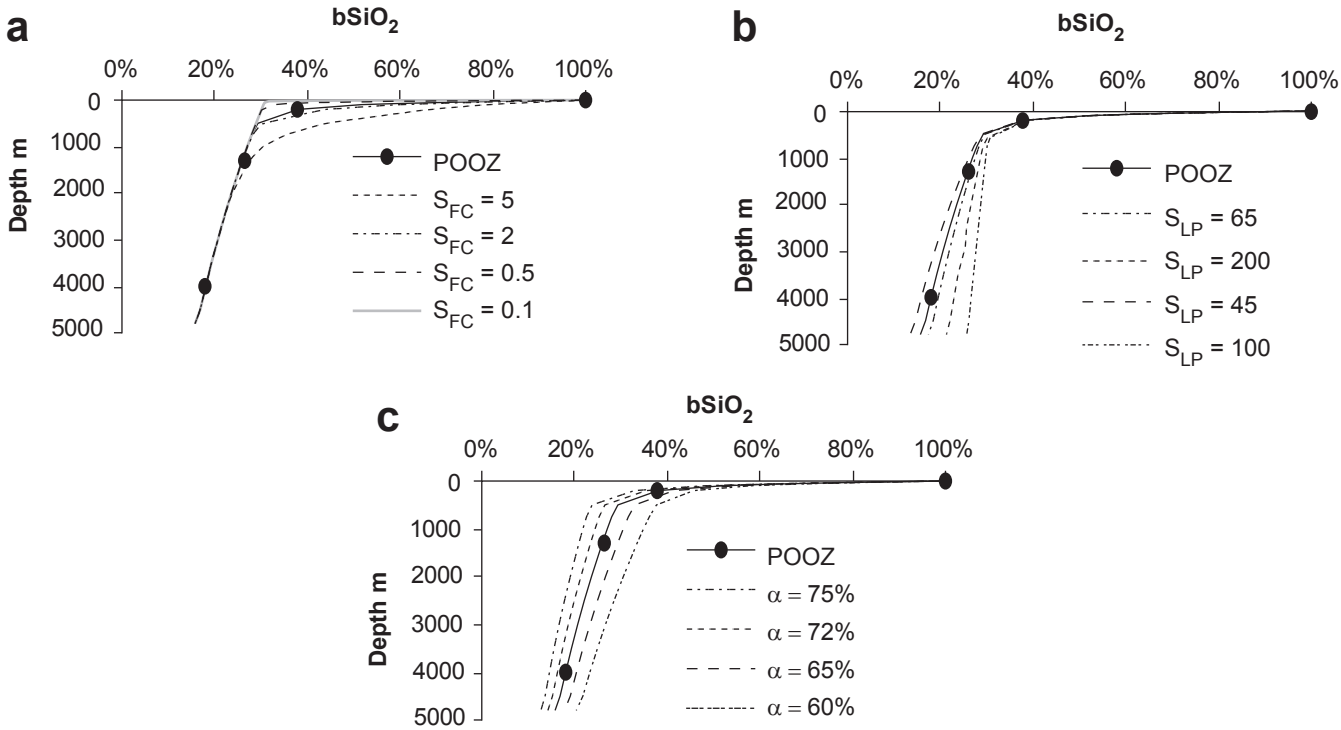
a
bSiO2
0%
20%
40%
60%
80%
100%
0
1000
2000
3000
4000
5000
Depth m
POOZ
SFC = 5
SFC = 2
SFC = 0.5
SFC = 0.1
b
bSiO2
0%
20%
40%
60%
80%
100%
0
1000
2000
3000
4000
5000
Depth m
POOZ
SLP = 65
SLP = 200
SLP = 45
SLP = 100
c
bSiO2
0%
20%
40%
60%
80%
100%
0
1000
2000
3000
4000
5000
Depth m
POOZ
α = 75%
α = 72%
α = 65%
α = 60%

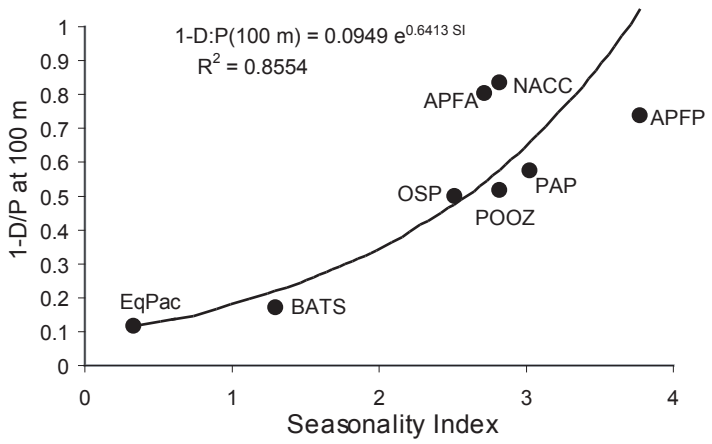
1-D:P(100 m) = 0.0949 e^0.6413 SI
R^2 = 0.8554
1-D/P at 100 m
Seasonality Index
0
0.1
0.2
0.3
0.4
0.5
0.6
0.7
0.8
0.9
1
0
1
2
3
4
EqPac
BATS
APFA
NACC
APFP
OSP
POOZ
PAP

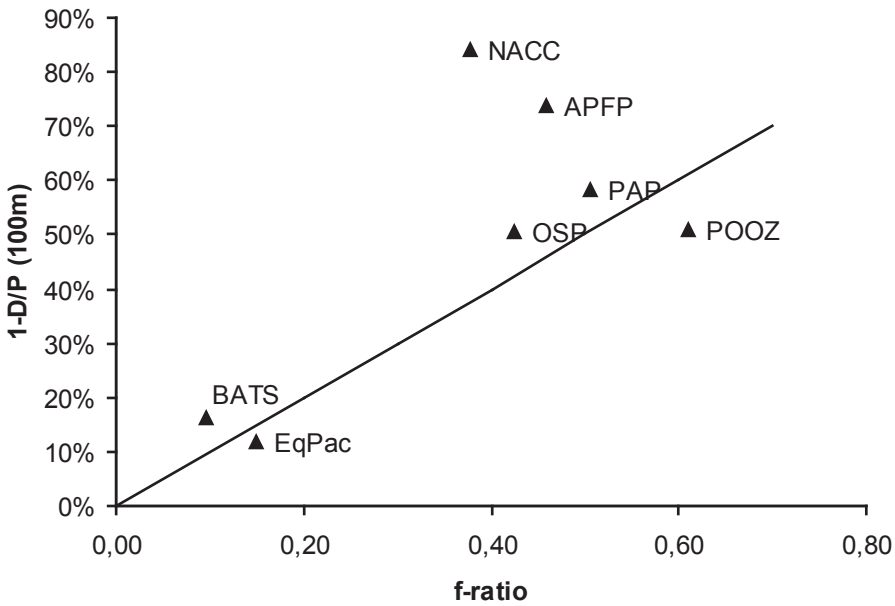
90%
80%
70%
60%
50%
40%
30%
20%
10%
0%
1-D/P (100m)
NACC
APFP
PAP
OSP
POOZ
BATS
EqPac
0,00
0,20
0,40
0,60
0,80
f-ratio

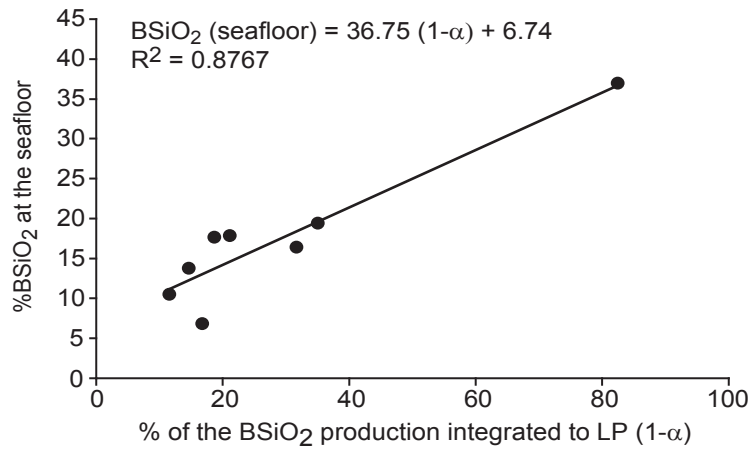
BSiO2 (seafloor) = 36.75 (1-α) + 6.74
R2 = 0.8767
%BSiO2 at the seafloor
% of the BSiO2 production integrated to LP (1-α)
0
5
10
15
20
25
30
35
40
45
0
20
40
60
80
100